

STATUS OF DATA PROCESSING AND ANALYSIS PREPARATION FOR THE ACES MICROWAVE LINK

F. Meynadier¹, P. Delva¹, C. Le Poncin-Lafitte¹, P. Laurent¹ and P. Wolf¹

Abstract. Our team in SYRTE-Observatoire de Paris is currently working on a software prototype for the processing and analysis of the data coming from the microwave link of the ACES (Atomic Clocks Ensemble in Space) mission. The goal of the mission is to realize, in space, a very accurate and highly stable time scale that will be compared to ground clocks. A critical part of this project is the time and frequency transfer between the ground and space stations: this will rely heavily on the microwave link, so it is critical to find a robust and accurate algorithm for this task.

Keywords: Atomic clocks, time transfer, fundamental physics experiments.

1 Introduction

The Atomic Clocks Ensemble in Spaces (ACES) mission is an international metrological space mission that will provide a highly stable and accurate time scale in space, by sending a caesium atom clock on board of the International Space Station (Salomon et al. 2007). A basic description of the time transfer mechanism as already been presented as a poster during the previous «Journées de la SF2A» (Meynadier et al. 2011). This presentation focusses on the current status of our study on the data processing and analysis.

2 Performance goals

The objective of the mission is to reach, for the clocks ensemble, a relative frequency stability (ADEV) of $\sigma_y = 10^{-13}\tau^{-\frac{1}{2}}$ (i.e. 3×10^{-16} after one day of integration, see Fig. 1), and a TDEV better than $2.1 \times 10^{-14}\tau^{-\frac{1}{2}}$ (i.e 12 ps after one day of integration, see Fig. 2), with an absolute frequency accuracy around 10^{-16} .

This translates to constraints on the microwave link stability: when comparing ground clocks to on-board clock while both ground station "see" the ISS (common view mode), the stability should be around 0.3 ps after 300 s of integration. For clock comparison through successive, non-overlapping comparison with the on-board clock (non-common view mode), it should stay within 7 ps after one day of integration. In practice, the signal will consist in pseudo-random noise which will be used to encode the date: once correlated with locally produced code it will provide a «code phase» measurement, but it will also possible to use the carrier phase for finer (albeit ambiguous) measurement.

3 Time transfer method

The desynchronisation between two clocks g and s is the proper time difference between those two clocks at a given coordinate time, $\tau^s(t) - \tau^g(t)$ (in what follows, proper times will be noted τ with a superscript denoting which clock is considered, whereas t will denote coordinate times). We can measure this by continuously encoding the proper time of clock g in a signal, send it to clock s , and then measure clock s proper time interval between the reception of the signal and the local occurrence of the same proper time. However this value will include the signal's time of flight and various internal delays, and care should be taken to convert them from proper time to coordinate time.

¹ LNE / Syrte – Observatoire de Paris, CNRS, UPMC Univ Paris 06, UMR8630, F-75005, Paris, France

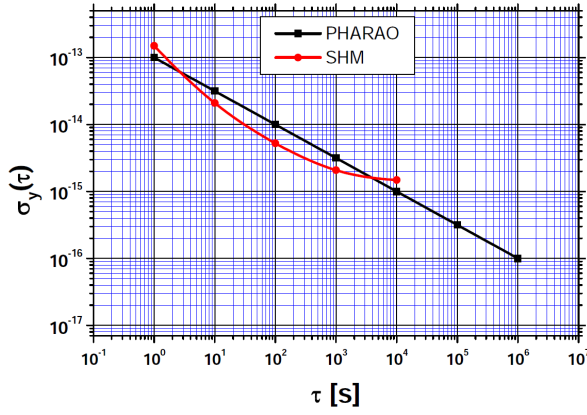


Fig. 1. PHARAO (Cesium clock) and SHM (hydrogen maser) expected performances in Allan deviation.

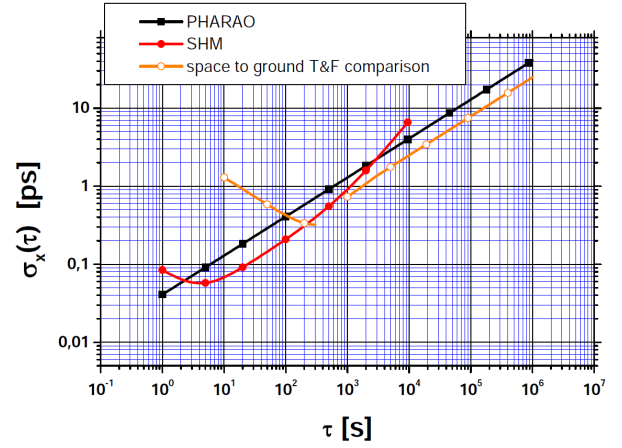


Fig. 2. Performance objective of the ACES clocks and the ACES space-ground time and frequency transfer expressed in time deviation.

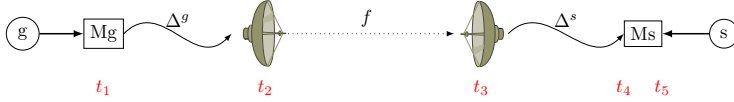


Fig. 3. Sequence of events for a one-way time transfer.

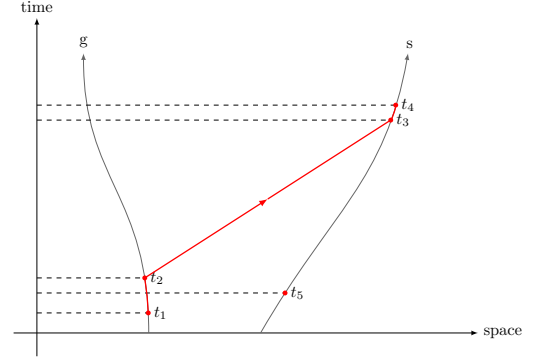


Fig. 4. Corresponding space-time diagram.

A conventional way to represent this "one-way" measurement is shown on Fig.3 and 4. With those conventions, it is assumed that

$$\tau^g(t_1) = \tau^s(t_5) \quad (3.1)$$

i.e. the ground clock at coordinate time t_1 displays the same proper time as the space clock at coordinate time t_5 . Then the signal from the ground clock travels to the emitting dish and reaches it at t_2 . It will reach the receiving dish at t_3 , and will finally arrive at the on-board comparator at t_4 . We define

$$\Delta\tau^s(\tau^s(t_4)) = \tau^s(t_5) - \tau^s(t_4) \quad (3.2)$$

as our observable: it is the difference of proper time between the reception of a particular time code and its local production, which is susceptible of varying with the clock's proper time.

What we are looking for is the desynchronisation between the two clocks at t_4 , i.e. in this case $\tau^s(t_4) - \tau^g(t_4)$. We will link this expression to the $\Delta\tau$ observable: for clarity we'll introduce the following notations: $T_{ij} = t_j - t_i$ and $[\cdot]$ for coordinate to proper time transformation (and back), a superscript indicating what transformation is performed. We also note $\Delta^g = [T_{12}]^g$ and $\Delta^s = [T_{34}]^s$, respectively, the internal delays caused by ground and space terminal.

We can then write:

$$\tau^s(t_4) - \tau^g(t_4) = -\Delta\tau^s(\tau^s(t_4)) - [T_{23} + [\Delta^g + \Delta^s]^t]^g \quad (3.3)$$

$$(3.4)$$

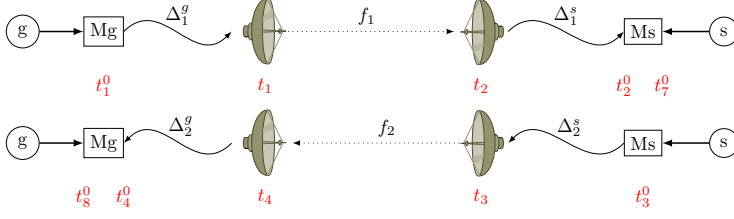


Fig. 5. Sequence of events for a two-way time transfer.

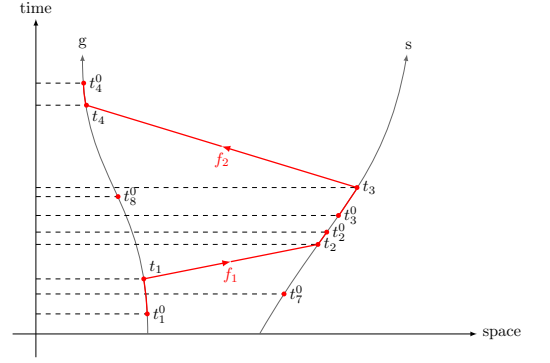


Fig. 6. Corresponding space-time diagram.

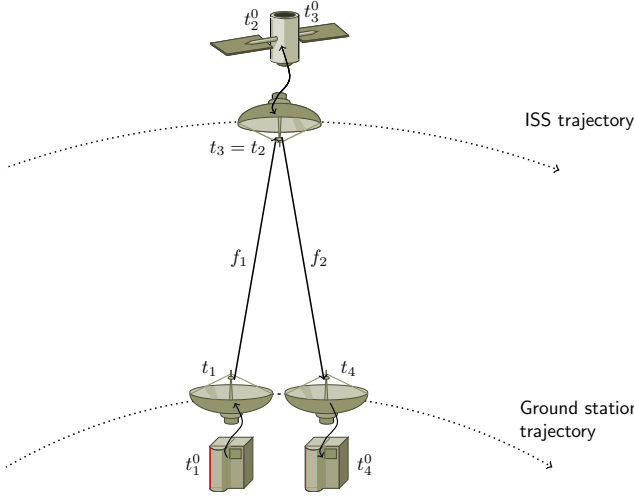


Fig. 7. Lambda configuration schema. As the ISS is supposed to be at the same point of the trajectory upon uplink signal reception and downlink signal emission, uncertainties on orbitography cancel out at the first order.

The two-way measurement is in fact a combination of two one-way measurements: such a measurement is presented on Fig. 5 and 6.

Following the same reasoning as for one-way measurements, we can get two expressions for the desynchronisation and use it to cancel most of the time-of-flight term, which is the main source of uncertainty:

$$\tau^s(t_1^0) - \tau^g(t_1^0) = \frac{1}{2} \left[[\Delta\tau_{\text{mo}}^g(t_4^0) - \Delta\tau_{\text{mo}}^s(t_2^0)]^t + T_{34} - T_{12} \right]^s \quad (3.5)$$

where $\Delta\tau_{\text{mo}}$ stands for the "modified" observable, corrected for the internal delays (i.e. $\Delta\tau_{\text{mo}} = \Delta\tau + \Delta^g + \Delta^s$).

We can even go further towards uncertainties minimization by choosing $t_2 = t_3$. This does not happen in principle, as each link's measurements are integrated over a 80 ms period which has no reason to be the synchronised on board and on ground. But we can always interpolate either downlink or uplink measurement to reach this configuration, dubbed the "Λ-configuration" (see Fig. 7).

Signal propagation is affected by the troposphere and the ionosphere, the former being modelised as a (mostly) non-dispersive medium, and the latter, which has a frequency dependant effect, being determined thanks to measurements of a secondary downlink with a much lower frequency. As it is necessary to calculate the Total Electron Content as an intermediate result for computing those delays, we'll issue the TEC as one of the scientific products of the ACES measurements.

More detailed developments of the calculations, with discussion of the various effects, can be found in Delva et al. (2012).

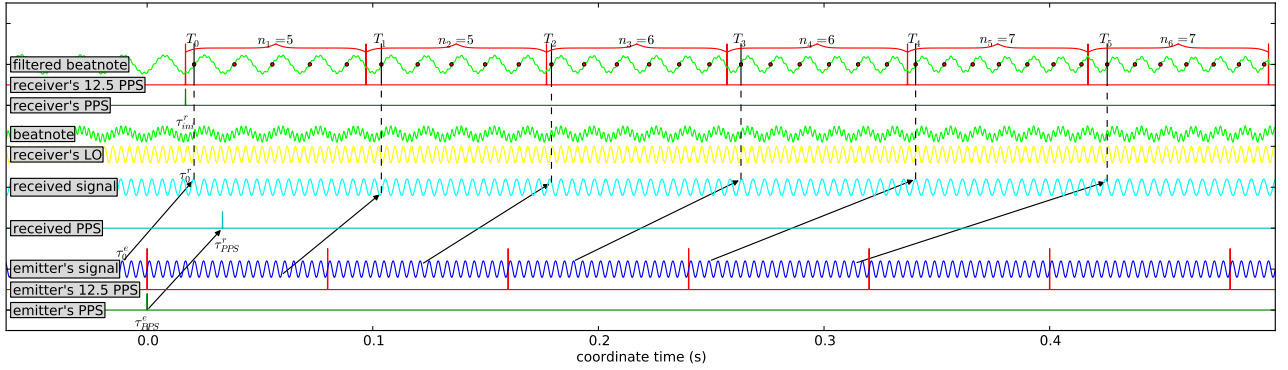


Fig. 8. From bottom to top, various steps for the generation of the data.

4 Recovering $\Delta\tau$ from hardware data

As we have seen our basic assumption is that we have access to the $\Delta\tau$ observables to get back to the desynchronisation. Unfortunately we do not have direct access to such data, and the last few months has been devoted to the recovery of $\Delta\tau$ observables (Syrté Team, or ST observables) from what the hardware gives us access to (TimeTech, or TT observables hereafter). TimeTech hardware shapes both code-phase and carrier-phase measurements the same way: they are materialized by a periodic signal which is locked on the measured phase.

Figure 8 summarizes our understanding of the measurement. It can roughly be read from bottom to top:

- The 3 bottom curves represent the emitter's time scales: 1 Pulse Per Second signal in green, a 12.5 Hz pulses that delimit the 80 ms period in red, and a blue sine wave which represents the either the code or the carrier phase that is sent through the emitter's dish.
- The "received PPS" and "received signal" represent how those signals are received with a variable delay (mostly due to the relative motion of the receiver, but it also includes all kind of delays encountered during the signal's transmission here). The propagation delay is represented by the black arrows.
- The yellow sine wave is the receiver's local oscillator: its frequency is close enough to be mixed with the incoming carrier signal and generate a beatnote (green signal above).
- The beatnote is then filtered (top green curve) and measured against the receiver's PPS and 12.5 PPS. For each 80 ms sequence, two numbers are generated: the number of ascending zero-crossing of the beatnote during the previous interval (n_m , materialized by red dots here) and the value of the local timer (T_m) at the moment when the first zero-crossing of the sequence (this timer has a roughly 10 ns resolution).

One should note that

- The number of zero-crossings is not constant throughout the measurements when the relative speed between the emitter and the receiver varies sufficiently.
- A beatnote zero-crossing does not necessarily corresponds to a carrier phase zero-crossing, which forbids direct relation between the two.

What is foreseen to be retrieved from the raw telemeasure is a list of T_m and n_m with time tags, forming what we call the «TT observables». The relation between the ST and the TT observables is iterative:

$$\Delta\tau_m(T_m) = \Delta\tau_{m-1}(T_{m-1}) + \left(\frac{\omega_{L.O.}}{\omega_e} - 1 \right) (T_m - T_{m-1}) \pm \frac{2\pi n_m}{\omega_e} \quad (4.1)$$

Equation (4.1) can be interpreted as follows: from one sequence to the next, the $\Delta\tau$ changes if the proper time interval $T_m - T_{m-1}$ is different to the proper time interval corresponding to n_m cycles of the carrier, with a $\frac{\omega_{L.O.}}{\omega_e} - 1$ factor converting the (integer) number of beatnote cycles to the (possibly non-integer) number of carrier cycles. The \pm in front of the last term accounts for a technical difference between code phase and carrier

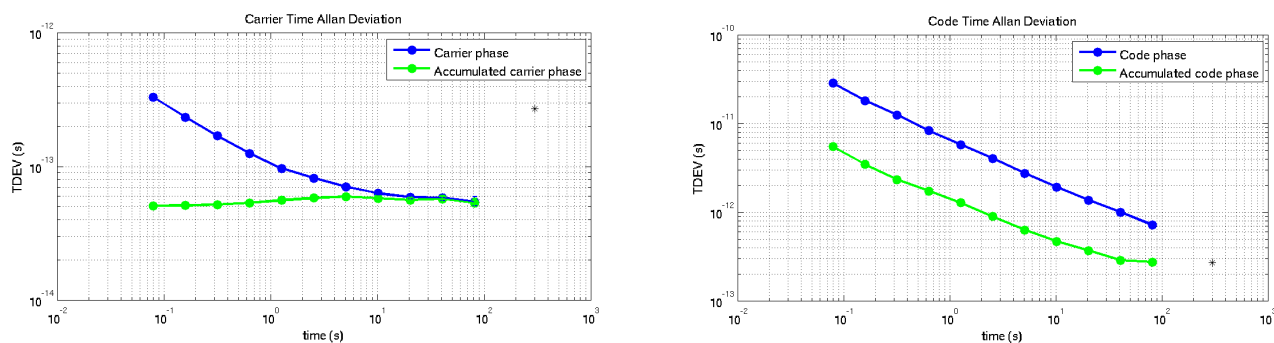


Fig. 9. Short term stability (TDEV) of ST observables, derived from carrier phase (**left**) or code phase (**right**) measurements, for both “phase” and “accumulated phase” observables.

phase measurements: in one case the local oscillator’s frequency is higher than the incoming signal, and in the other case it’s the opposite, thus changing the sign of $\frac{\omega_{L.O.}}{\omega_e} - 1$: the $\frac{2\pi n_m}{\omega_e}$ term must have the opposite sign to compensate.

Then, we determine the initial term by using the fact that the PPS signal is unambiguous: the desynchronisation plus the propagation time will always be, in our case, of the order of a few milliseconds, so we can safely assume that the «received» PPS will always be close to the «receiver’s» PPS, the interval between the two giving us a rough estimate of the $\Delta\tau_0$. By exploiting the fact that the emitted PPS is phase-coherent with the signal, we can even reach an absolute accuracy better than 100 ps on $\Delta\tau_0$ and we are currently working on a method to achieve the necessary accuracy to «bridge the gap» from one ISS transit to the next. This method relies on an additional observable, the «accumulated phase», which represents the same observable as the regular phase, but overcomes the reading uncertainty by averaging intermediate values. Figure 9 shows how much the use of «accumulated phase» observables will enhance the stability of our measurements.

5 Simulation

In parallel to the development of the data processing software, our team is developing an independent simulation software which already provides valuable data and allows to test the processing software modules. Currently implemented are:

- ISS orbitography + ground stations coordinates in ITRF, with transformation into ICRF
- Clock modelisation for ISS & ground stations, with basic noise simulation.
- Time transfer modelisation between the two terminals
- Generation of TimeTech observables, together with theoretical values against which calculated values will be compared.

A first step is to check that our pre-processing software correctly reconstructs the $\Delta\tau$ observables: an example of such a comparison is displayed on Fig. 10. This figure also illustrates the difference between carrier phase and code phase measurements: in this simulation, carrier phase data has a small dispersion (typically 0.5 ps) but a large offset with respect to the theoretical values (here, 1740 ps) whereas code phase data has around 20 ps dispersion but has a mean offset of a few ps.

Simulation software is also useful to evaluate the impact of each effect in the overall delay: figure 11 shows how several delays vary during one simulated ISS transit.

6 Conclusion

The ACES MWL data processing is still in development, but some major hurdles have been overcome this year. We have already started to implement the algorithm described by Duchayne (2008) and hope to have a working software prototype in the near future.

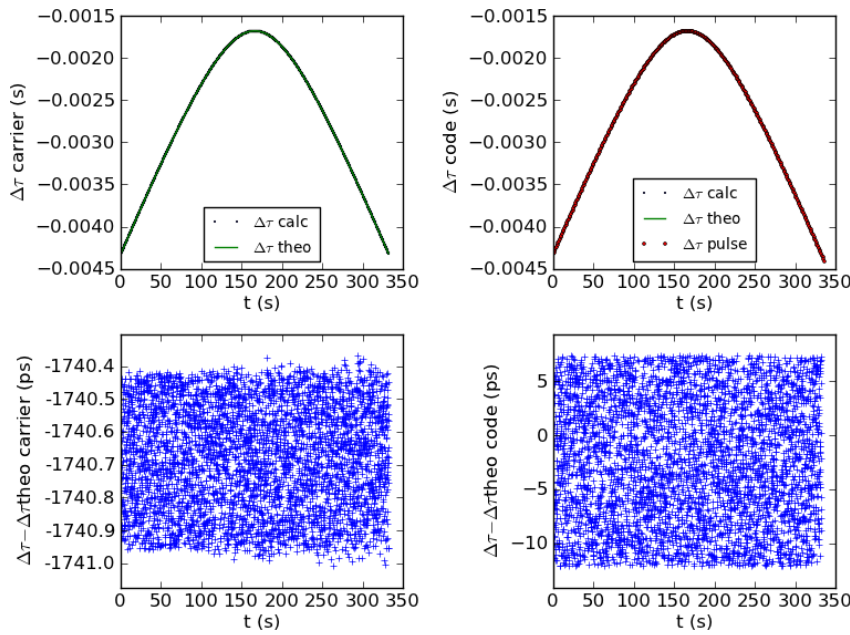


Fig. 10. Preprocessing software: comparison between ST observables calculated from simulated TT observables, and theoretical ST observables, for carrier (left) and code (right).

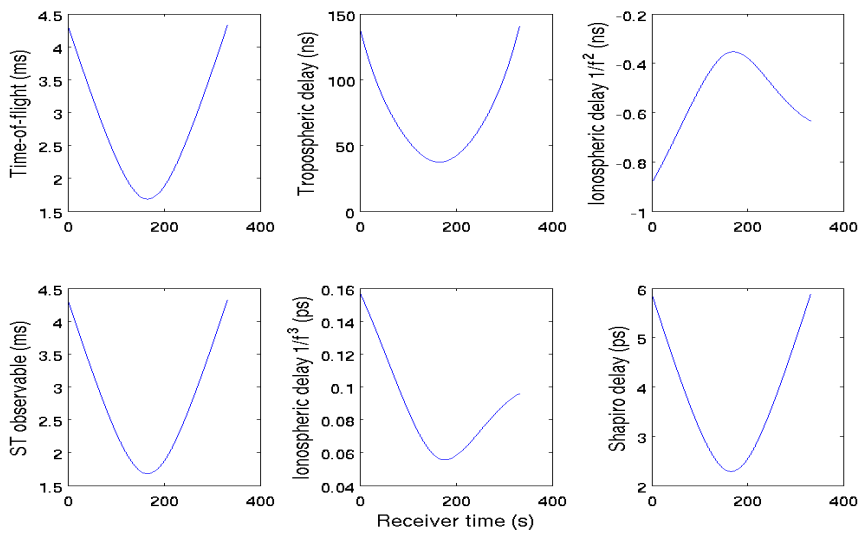


Fig. 11. Delays induced by several effects during one simulated transit, and corresponding ST observable. The main source of delay is the geometrical time of flight, followed by the tropospheric delay. The ionospheric delay is decomposed in terms of $1/f$ dependency, the second order being dominant.

References

- Delva, P., Meynadier, F., Wolf, P., Le Poncin-Lafitte, C., & Laurent, P. 2012, ArXiv (1206.6239)
- Duchayne, L. 2008, PhD thesis, Observatoire de Paris, France
- Meynadier, F., Delva, P., Le Poncin-Lafitte, C., Laurent, P., & Wolf, P. 2011, in SF2A-2011: Proceedings of the Annual meeting of the French Society of Astronomy and Astrophysics, ed. G. Alecian, K. Belkacem, R. Samadi, & D. Valls-Gabaud, 679
- Salomon, C., Cacciapuoti, L., & Dimarcq, N. 2007, International Journal of Modern Physics D, 16, 2511